Thermochimica Acta 511 (2010) 43–50

Contents lists available at ScienceDirect

Thermochimica Acta

journal homepage: www.elsevier.com/locate/tca

Temperature and composition-dependent properties of the two-component system D- and L-camphor at 'ordinary' pressure

Ivo B. Rietveld[a,*], Maria Barrio[b], Nestor Veglio[b], Philippe Espeau[a], Josep Lluis Tamarit[b], René Céolin[a,b]

[a] Département de Physico-chimie du Médicament, EAD Physico-chimie Industrielle du Médicament (EA4066), Faculté de Pharmacie, Université Paris Descartes, 4 Avenue de l'Observatoire, 75006 Paris, France
[b] Grup de Caracterització de Materials (GCM), Departament de Física i Enginyeria Nuclear, Universitat Politècnica de Catalunya, ETSEIB, Diagonal 647, 08028 Barcelona, Spain

ARTICLE INFO

Article history:
Received 12 May 2010
Received in revised form 20 July 2010
Accepted 21 July 2010
Available online 30 July 2010

Keywords:
Phase diagram
Racemic compound
Fusion
Solid solution
Mixed crystals
Plastic crystals

ABSTRACT

The properties of dextrorotatory and racemic camphor have been investigated as a function of temperature and composition. A thorough literature survey has been undertaken for temperatures and enthalpies of all transitions and for structural information of the phases existing under ordinary pressure. The transition temperatures and enthalpies have been measured with differential scanning calorimetry. Cell parameters of all phases have been determined as a function of temperature up to the melt and the specific volume of liquid camphor has been determined. A temperature–composition phase diagram is presented containing all condensed-phase transitions, including an analysis of the melting transition. The melting point of racemic camphor is at least 2 K lower than the melting point of D- (and L-) camphor at 451 ± 2 K, whereas the melting enthalpy is the same within error. Below the melting point, mixtures of solid D- and L-camphor are solid solutions. Because the structures of the racemic compound near the melting point and the solid solution are equivalent for time and volume averaged measurements, they cannot be distinguished. One could call this a case of 'critical symmetry'.

1. Introduction

1.1. General introduction

Phase behavior of binary mixtures has always received a lot of attention, not only to improve academic understanding but also for industrial applications, including in pharmacy. As for systems of optically active substances, a comprehensive treatise about their thermodynamic behavior appeared in 1981 written by Jacques et al. [1] Enantiomer mixtures behave different from pure substances, which can be demonstrated with temperature–composition (*T*–*X*) phase diagrams (*X*: composition in mole fraction).

Since camphor is known for centuries, its phase behavior was assumed to be well understood. However, after examination of its solid-state properties in the literature, basic data at 'ordinary' pressure surprisingly appeared to be either questionable or even lacking. The low-temperature binary phase diagram of camphor has received a fair amount of attention, in particular its solid–solid transitions [2–6]. Open questions are whether D-camphor and racemic DL-camphor have different melting points and different melting enthalpies. This would complete the phase diagram of the condensed phases presented by Mjojo and Schäfer and Wagner [3,6]. In addition, the evolution of the specific volume for D-camphor and for the racemic mixture have been studied from 100 K to their respective melting points and beyond into the melt. Although certain aspects of the low-temperature transition (phase III–phase II) of DL-camphor remain unclear [4,7,8], it falls outside the scope of this paper.

Finally, in this paper the word 'transition' is used in the sense of a reversible shift from one phase to another, hence while the two phases are in equilibrium. This has been done for the sake of brevity, even though the general meaning of the word (phase-) 'transition' also includes irreversible phase shifts.

1.2. Literature survey

1.2.1. The camphor molecule

The molecular formula of camphor was determined in 1833 but it took another 60 years before Julius Bredt proposed the correct structure in 1893 [9]. Camphor, a bicyclic monoterpene (1,7,7-trimethyl-bicyclo(2,2,1) heptan-2-one), exhibits two asymmetric carbon atoms (Fig. 1). Dextrorotatory camphor is made of molecules with the absolute configuration *R*, (1*R*,4*R*)-(+)-camphor (CAS No. 464-49-3), and levorotatory camphor is (1*S*,4*S*)-(−)-camphor (CAS No. 464-48-2). 4*R* and 4*S* are often omitted. Pure dextrorotatory camphor (D-camphor, $C_{10}H_{16}O$, $M = 152.2334\ g\ mol^{-1}$) is produced naturally by the camphor tree and other plants and so is lev-

* Corresponding author. Tel.: +33 153739675.
E-mail address: ivo.rietveld@parisdescartes.fr (I.B. Rietveld).

0040-6031/$ – see front matter © 2010 Elsevier B.V. All rights reserved.
doi:10.1016/j.tca.2010.07.023

Table 1
Crystallographic data from the literature for D- and DL-camphor.[a]

Phase	Lattice parameters			Z	V (Å^3)	T (K)	Ref.
	a (Å)	b (Å)	c (Å)				
D-Camphor							
III, orthorhombic $P2_12_12_1$	8.9277	27.0359	7.3814	8	1781.64	100	[12]
II, hexagonal (OD)	7.14		11.72	2	517	295	[3,7]
I, face-centered cubic (OD)	10.1			4	1030	380	[3]
DL-Camphor							
III, orthorhombic *Cmcm*	6.8341	11.6584	11.5000	4	916	100	[8]
II, hexagonal (OD)	7.05		11.50	2	476	295	[3]

[a] Z: number of molecules in unit cell, V: unit cell volume, T: measurement temperature, OD: orientationally disordered.

Table 2
Transition temperatures and enthalpy changes of D-camphor (in part based on Ref. [13]).

III → II		II → I		I → liquid		Ref.
T (K)	ΔH (kJ mol^{-1})	T (K)	ΔH (kJ mol^{-1})	T (K)	ΔH (kJ mol^{-1})	
				450.8	6.0	[36]
245		370				[10]
		360.2	0.106			[37]
–	7.78 ± 0.08					[33,38]
		332 ± 28	0.4 ± 0.4[a]	453 ± 25	6.5 ± 0.3[a]	[24]
243	6.99 ± 0.15	374.2	0.234 ± 0.024	452	6.862	[5,6]
243.8 ± 0.1	6.99 ± 0.15					[38,39]
245.0	11.49					[40]
245				449		[41]
243	10.65					[42]
242 ± 1	16 ± 1[b]					[3]
244	11.3 ± 0.8			450	5.4 ± 0.4	[43]
				452.2		[44]
				447–448		[45]
				453.2		[46]
244.19	7.600[c]	371.66	0.218[c]			[4]
				462.3 ± 0.5	15.7 ± 0.6	[14,38]
				449.8–451.9	6.0 ± 0.2	[16]
				451.75		[13][d]
				451.95		[13][d]
				451.95		[13][d]
				451.75		[15]
244 ± 1	10 ± 3	369 ± 6	0.19 ± 0.07	451 ± 2	6.2 ± 0.6	Average[e]

[a] Calculated by fitting of sublimation and vaporization data, see also text.
[b] Mjojo states that the enthalpy value is unreliable [3].
[c] Estimates by Witusiewicz et al. [13] using heat capacity data of Nagumo et al. [4].
[d] References found in Ref. [13] of which an original document could not be obtained: 451.75 K (Haller, 1882), 451.95 K (Louqinine, 1889), and 451.95 K (Fancone, 1912).
[e] Data of De Wilde [24] not used for the average of the II-I transition and data of Donnelly et al. [14] not used for I–L average.

Table 3
Transition temperatures and enthalpies of DL-camphor.

III → II		II → I		I → liquid		Ref.
T (K)	ΔH (kJ mol^{-1})	T (K)	ΔH (kJ mol^{-1})	T (K)	ΔH (kJ mol^{-1})	
		367				[10]
				440.6–446.1	5.6 ± 0.2	[16]
210	0.84			452	6.862	[5]
210 ± 1	0.84 ± 0.03					[39]
203.6	2.23					[40]
203.8	0.72	350	0.234 ± 0.024			[6]
				451.6	6.82 ± 0.03	[38,47][a]
				451.75		[15]
206 ± 1	1.9[b]					[3]
206				451		[41]
218.2	0.98[c]					[4] Annealed
209.12	1.2[c]	367[c]	0.24[c]			[4] Rapidly cooled
203.8		350		449		[48]
207 ± 3[d]	1.2 ± 0.6	358 ± 10	0.237 ± 0.004	450 ± 4	6.4 ± 0.7	Average

[a] Frandsen [47] uses the phrase 'synthetic camphor', which implies DL-camphor, in the table in Ref. [13] it was grouped with D-camphor.
[b] Mjojo [3] states that the enthalpy value is unreliable.
[c] Values determined from data available in Ref. [4].
[d] Average of unannealed samples.

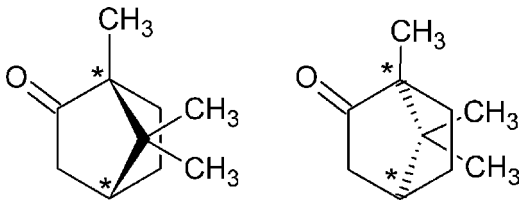

Fig. 1. D-Camphor (absolute configuration *R*) and L-camphor (absolute configuration *S*) molecules (*asymmetric carbon atoms).

orotatory camphor (L-camphor), while synthesis yields racemic DL-camphor (CAS No. 76-22-2).

1.2.2. Crystallographic data

In 1914, Wallerant observed that D-camphor forms rhombohedral crystals at room temperature and cubic crystals above 370 K [10]. At 245 K, he observed that the D-camphor rhombohedral crystals transformed into another rhombohedral crystal. Furthermore, he reported that DL-camphor consists of rhombohedral crystals at room temperature, becomes cubic at 367 K, and does not exhibit a transition at 245 K.

In accordance with the observations of Wallerant, three solid phases are known for D-camphor at ordinary pressure (Table 1). The high- and room-temperature phases, cubic (I, 369–451 K) and hexagonal (II, 244–369 K), respectively, are orientationally disordered phases (plastic phases or rotator phases). The low-temperature phase, orthorhombic (III, <244 K), is a regular crystal without rotational freedom.

DL-Camphor possesses structures with the same basic symmetry: face-centered cubic, hexagonal, and orthorhombic, only the transition temperatures tend to differ from those of D-camphor. The low-temperature orthorhombic phase (<207 K) of DL-camphor is highly disordered [4,8,11]. Its crystal structure has only recently been determined and it was found to be different from the orthorhombic structure of D-camphor (Table 1) [8,12]. This defines orthorhombic DL-camphor as a racemic compound. For the high-temperature cubic phase (from 358 K to 449 K) of DL-camphor, no lattice parameters were found in the literature. Both the cubic and the hexagonal phases are orientationally disordered and it is not yet understood how this affects the presence of a racemic compound. The available crystallographic data are compiled in Table 1. The roman numerals I–III will be used as shorthand for, respectively, the cubic, hexagonal and orthorhombic solid phases, L stands for liquid phase and v for the vapor phase.

1.2.3. Calorimetric data concerning D-camphor

Recently, a large number of transition temperatures and enthalpies of D-camphor were compiled by Witusiewicz et al. [13] Table 2 consists of those and additional data found in the literature. One can observe that for the two transitions at about 244 K and 451 K there is a good agreement between the reported transition temperatures. For the transition enthalpies and for the third transition, however, there are significant discrepancies between the reported values. Averaging the melting enthalpy, while eliminating the value determined by Donnelly et al. [14], leads to an average value of $6.2 \pm 0.6\,\mathrm{kJ\,mol^{-1}}$.

1.2.4. Calorimetric data concerning racemic camphor

In Table 3, transition data from the literature are compiled for DL-camphor. The scatter over the transition data is as large as for D-camphor. The III → II transition was meticulously studied by Nagumo et al. and they concluded that the transition temperature depends on the extent of disorder in the orthorhombic phase [4]. In their paper, it is reported that the disordered orthorhombic crystal has a transition temperature of 209.12 K, and in the case of samples annealed for a month, the transition temperature is found at 218 K [4]. The melting temperatures of D-camphor and racemic camphor do not differ according to Schäfer and Frey and neither do their enthalpies [5]. Also Ross and Somerville do not find a difference in melting points [15]. Abrosimov et al. find a significant difference in melting enthalpies and temperatures [16]. The average melting points and melting enthalpies for D- and DL-camphor are the same within error (Tables 2 and 3), 451 ± 2 K, $6.2 \pm 0.6\,\mathrm{kJ\,mol^{-1}}$ and 450 ± 4 K, $6.4 \pm 0.7\,\mathrm{kJ\,mol^{-1}}$, respectively. If the average is taken over all melting points found by the ACS Sci-Finder (experimental properties) for DL-camphor and D-camphor (the latter in combination with L-camphor), one obtains, respectively, 449 ± 5 K and 451 ± 3 K. Again, D-camphor has a slightly higher melting point, but within error, the values are the same. Thus, despite the abundance of data, questions remain whether DL-camphor and D-camphor have different melting points and different enthalpies of fusion and which consequences this entails.

The present paper does not claim to present the ultimate melting point of D-camphor and its racemic mixture, but the idea is to present a large number of measurements for both D- and DL-camphor, performed on the same DSC (differential scanning calorimeter) to determine whether the result is different statistically and to study the consequences in the binary system.

1.3. Determination of transition enthalpies for substances with a non-negligible vapor pressure

One of the reasons for the uncertainty of the enthalpy of fusion may be camphor's vapor pressure. Substances with a non-negligible vapor pressure will partially evaporate during a heating run in a DSC apparatus and fill up the dead volume of the DSC pan. It is in general impossible to determine the heat of vaporization involved, because evaporation is the result of a shifting monovariant equilibrium with temperature and it will therefore displace the baseline. Obviously, it will also diminish the amount of material available for fusion and thus decrease the recorded transition enthalpy. This effect can often be neglected, but for substances with a considerable vapor pressure, it may have to be taken into account. One can try to fill the pan completely, but this is often impractical and may result in badly closing lids. Alternatively, vaporization can be accounted for by determining the apparent melt enthalpy as a function of V/m, with V the inner volume of the pan and m the initial mass of the specimen. V/m is in fact the specific volume, v_{spec}, of the heterogeneous substance in the DSC pan. Extrapolation to $V/m \approx 0$ or 1 (since the v_{spec} of the condensed phases are close to $1\,\mathrm{cm^3\,g^{-1}}$ for organic molecular compounds) should lead to a more realistic value for the enthalpy of fusion. The method has been applied previously to adamantane and to arsenic [17,18].

2. Materials and methods

2.1. Chemical compounds

DL-Camphor was purchased from Sigma–Aldrich (France) (>98%) while D-camphor was obtained from Prolabo (France) (>97%). All batches were used as such. Camphor sublimed under a temperature gradient was used for verification.

2.2. Calorimetry

Differential scanning calorimetry (DSC) experiments were performed using a Mettler-Toledo (Switzerland) 822e thermal analyzer equipped with a Huber (Germany) TC100 cooling device for measurements down to 190 K. Indium ($T_{fus} = 429.75$ K, $\Delta_{fus}H = 3267\,\mathrm{J\,mol^{-1}}$) and zinc ($T_{fus} = 692.68$ K,

$\Delta_{fus}H = 7320\,J\,mol^{-1}$) were used for calibration of temperature and transition enthalpies [19].

A second series of measurements for both D- and DL-camphor was conducted with a Q100 thermal analyzer, from TA Instruments (USA). Specimens were weighed using microbalances sensitive to 0.01 mg and sealed in aluminum pans. For quantities smaller than 1 mg a TGA-thermobalance from Mettler-Toledo (Switzerland), sensitive to 0.001 mg, was used. DSC runs were performed at heating rates ranging from 1 K min^{-1} to 20 K min^{-1}.

2.3. High resolution X-ray powder diffraction

For the cell parameters of the camphor system under various conditions, high resolution X-ray measurements were performed on two transmission mode diffractometers using Debye–Scherrer geometry equipped with horizontally mounted INEL cylindrical position-sensitive detectors (CPS-120) containing 4096 channels (0.0291° 2θ angular step) [20].

For measurements at room temperature a monochromatic Co-Kα1 (λ = 1.7889 Å) radiation was selected with an asymmetrically focusing incident-beam curved quartz monochromator. The generator power was set to 30 kV and 30 mA.

Measurements as a function of temperature were performed by means of a monochromatic Cu-Kα1 (λ = 1.5406 Å) radiation, selected with an asymmetrically focusing incident-beam curved quartz monochromator and with the generator power set to 35 kV and 35 mA. Temperature was controlled by means of a liquid nitrogen 700 series Cryostream Cooler from Oxford Cryosystems (United Kingdom).

External calibrations of both devices with cubic $Na_2Ca_3Al_2F_4$ were applied to convert the channels into 2θ-degrees by cubic spline fittings [21]. The Peakoc application in the Diffractinel software was used for the calibration as well as for the peak position determinations after pseudo-Voigt fittings; lattice parameters were refined with FullProf [22].

The samples were introduced in Lindemann capillaries (0.5-mm diameter) rotating perpendicularly to the X-ray beam during the experiments to improve the average of the crystallite orientation. For the temperature-dependent measurements in the range from 100 K up to the melting point, the sample temperature was equilibrated for about 10 min followed by an acquisition time for the OD phases of about 30 min and for phase III of ca. 1 h. The heating rate in between data collection was 1.33 K min^{-1}.

2.4. Specific volumes of liquid D-camphor and racemic camphor

Details on the method for the determination of the specific volume of molten compounds can be found in Ref. [23]. Accurately weighed quantities of D- and DL-camphor (masses of about 8 g weighed with a balance sensitive to 0.01 mg), respectively, were introduced in calibrated cylindrical silica tubes whose inner diameters of about 8 mm were accurately measured with an alesometer sensitive to 0.001 mm.

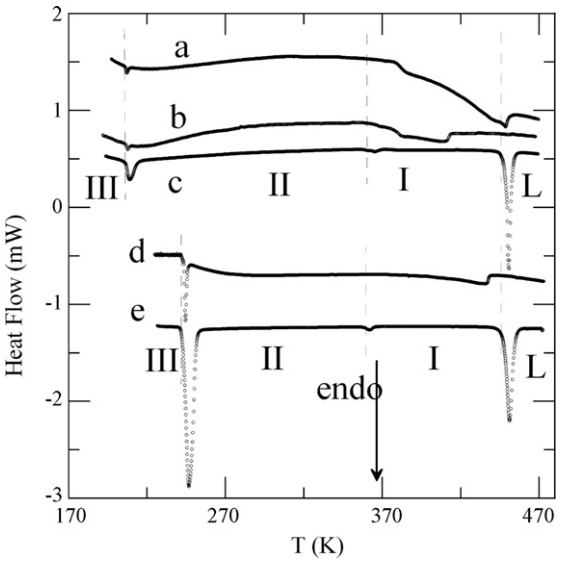

Fig. 2. Examples of DSC-curves exhibiting melting and/or sublimation phenomena. a (DL-Camphor): a large sublimation event visible from about 380 K with a small melting peak at 449 K. b (DL-Camphor): sublimation visible from 380 K, depleting solid camphor before melting takes place. c (DL-Camphor): regular melting peak at 449 K and the solid–solid transitions at 207 K and 358 K. d (D-Camphor): sublimation without clear onset, returning to baseline at 440 K and the solid–solid transition at 244 K. e (D-Camphor): melting peak at 451 and the solid–solid transitions at 244 K and 369 K; the intensity of the transitions causes the evaporation to fall onto the baseline.

After camphor had been cooled to about 210 K, each tube was sealed under a vacuum of 10^{-3} Pa. It was suspended in an XU 75/300 oven from Climats (France) whose temperature is controlled at ±1 K. The liquid was slowly heated or cooled and kept isothermally while the heights of the meniscus and of the flat bottom of the inner part of the tube were measured with a cathetometer accurate to 2 μm.

3. Results and discussion

3.1. Transitions of D-camphor and DL-camphor

Typical DSC-curves for camphor can be found in Fig. 2. The transition-related values, compiled in Table 4, coincide within error with those of the literature (Tables 2 and 3), except for the II → I transition of DL-camphor; however, the enthalpy of this transition is very small and the data in the literature is limited. The melting temperature of D-camphor is almost 4 K higher than the temperature of the racemic mixture, which is a small but statistically significant difference. The values have been determined over 53 and 36 separate samples, respectively, divided over two different DSC apparatuses.

3.2. Enthalpy of fusion as a function of V/m

The apparent enthalpy of fusion, $\Delta_{fus}H^*$, of D-camphor and of DL-camphor as a function of V/m decreases with an increase of dead volume in the pan (Fig. 3). It can be seen in Fig. 2, that this is caused

Table 4
Measured temperature and transition enthalpy of D- and DL-camphor transitions.

	T_{III-II} (K)	ΔH_{III-II} (kJ mol^{-1})	T_{II-I} (K)	ΔH_{II-I} (kJ mol^{-1})	T_{fus} (K)	$\Delta_{fus}H^a$ (kJ mol^{-1})	$\Delta_{fus}H^b$ (kJ mol^{-1})
D-Camphor	242.7 ± 0.6	11.2 ± 0.4	370 ± 4	0.16 ± 0.02	451.8 ± 0.7	6.3 ± 0.5	6.1 ± 0.5
DL-Camphor	206.1 ± 0.3	1.3 ± 0.3	364 ± 5	0.17 ± 0.02	448.0 ± 0.7	5.9 ± 0.2	6.0 ± 0.3

[a] Determined with average values of apparent $\Delta_{fus}H^*$ found with $V/m < 12$ cm^3/g.
[b] Determined by extrapolation of apparent $\Delta_{fus}H^*$ versus (V/m) to $V/m = 0$ (see text).

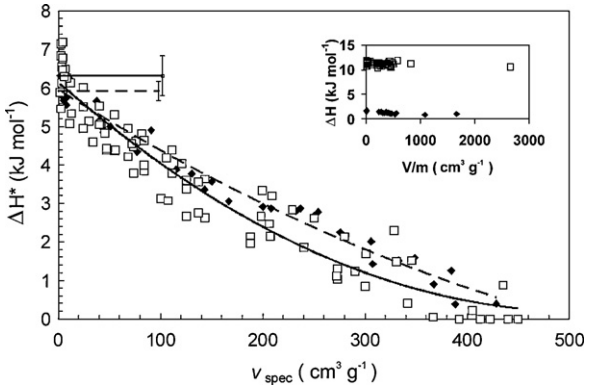

Fig. 3. The apparent enthalpy of fusion, ΔH^*, for D-camphor (open squares, solid line) and for DL-camphor (solid diamonds, broken line) as a function of the specific volume of the system (cf. text). The average over the values not exceeding 12 $cm^3\ g^{-1}$ is indicated with a straight line and an error bar. Inset: transition enthalpy of the III–II transitions for D- and DL-camphor.

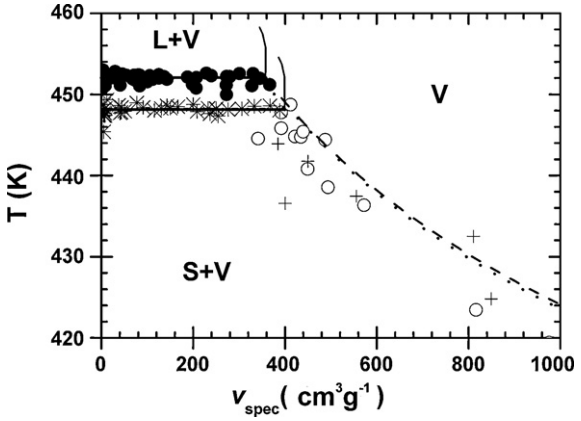

Fig. 4. The phase diagram of temperature versus specific volume of camphor. D-Camphor: '●' S–L–vap triple line and '○' S + vap → vap transition. DL-camphor: '*' S–L–V triple line and '+' S + vap → vap transitions. The straight lines are the average-melting-point invariants, i.e. the S–L–vap triple lines. The beginning of the bell-shaped curve representing the limit of the L + vap region has been indicated with a solid curved line. The dotted line is calculated assuming ideal behavior of the saturated vapor pressure of DL-camphor and using data from Ref. [24] (see also text). The broken line is obtained in the same way for D-camphor.

by sublimation. Curves 'c' and 'e' contain regular melting peaks, while curve 'a' exhibits sublimation with a leftover melting peak and curves 'b' and 'd' exhibit sublimation only, depleting the solid before melting can occur. Hence, camphor sublimes during a DSC heating run. The 7th column in Table 4 contains the average melting enthalpy of samples for which V/m does not exceed 12 $cm^3\ g^{-1}$ (marked in Fig. 3). The last column contains the values obtained by extrapolation of $\Delta_{fus}H^*$ to $V/m = 0$. For DL-camphor the result is the same, whereas for D-camphor there may be a decrease of 5% in comparison with the average in column 7; however, this falls within the measurement error, which is large: 10%. The large error may be due to uncertainties in the baseline, which may have several causes, including vaporization and differences in specific heat.

Extrapolating the curves in Fig. 3 to zero enthalpy (the regression results can be found in the supplementary materials), results in an estimate for the specific volume of the vapor: for D-camphor 488 $cm^3\ g^{-1}$ and for DL-camphor 501 $cm^3\ g^{-1}$. However, due to the small sample size at high V/m, the specific volume may be as low as 400 $cm^3\ g^{-1}$, which is where observable melting peaks cease to exist. With vapor-pressure data of D-camphor found in the literature [24], the specific volume can be calculated assuming perfect gas behavior; at their boiling points it leads to 495 $cm^3\ g^{-1}$ and 491 $cm^3\ g^{-1}$ for D- and DL-camphor, respectively. The calculated values indicate that the real values are probably lower than 490 $cm^3\ g^{-1}$, but that the estimates obtained by extrapolation are of the correct order of magnitude.

It is important to realize that the slope of $\Delta H_{III–II}$ as a function of V/m is zero within error for both D- and DL-camphor, because the vapor pressure at these much lower transition temperatures is negligible (cf. inset Fig. 3). This clearly indicates that V/m, or v_{spec} of the heterogeneous sample, is in fact a thermodynamic parameter and that one has to be aware of an increase of pressure in any sealed pan while running DSC experiments even if its influence is often negligible.

The melting temperature does not change with V/m, as can be seen in Figs. 2 and 4, but the melting event depends on the initial amount of camphor inside the DSC pan of fixed inner volume V. If the entire specimen sublimes before the melting point is reached, only a sublimation event is observed, which can be recognized as a return to the baseline in the DSC-curve (curve 'b' and 'd' in Fig. 2). The temperature of the end of sublimation depends on V/m (and on the DSC heating rate if the rate is too fast to maintain equilibrium).

Plotting the melting temperatures as a function of V/m one obtains an invariant line of the T–v_{spec} phase diagram (cf. Fig. 4) where v_{spec} is the specific volume of the heterogeneous mixture, i.e. independent of the number of coexisting phases. The straight lines in Fig. 4 represent the average-melting-point invariants or S–L–vap triple lines, because they connect the vapor phase on the right with the liquid and the solid phase, which both have specific volumes close to 1 $cm^3\ g^{-1}$.

The temperature related to the end of the sublimation event (cf. line 'd' and 'b' in Fig. 2) is marked in Fig. 4 with 'o' and '+' for D- and DL-camphor, respectively, and encloses the area where solid and vapor are in equilibrium. The curved broken lines on the right have been calculated with the vapor-pressure data published by De Wilde [24] assuming ideal behavior, although the calculated volumes of 495 $cm^3\ g^{-1}$ were shifted with −140 $cm^3\ g^{-1}$; evidently, the saturated vapor does not behave ideally. It can be seen that both lines closely connect the last measurable melting points of D- and DL-camphor. This is a strong indication that D- and DL-camphor exhibit almost the same vapor-pressure curve as a function of temperature. The broken lines roughly follow the points indicating the course of the S + vap → vap transitions. The scatter over the data is caused by uncertainties in the extreme small amount of camphor (high V/m) and in the inner volume of the pan.

Above the melting invariant line, there is a bell-shaped curve (not shown) enclosing the region where liquid and vapor coexist. It connects the specific volumes of the vapor and the liquid in equilibrium with each other through the critical point, which is the maximum of the bell-shaped curve. Points on this line could not be obtained due to its steep slope and high pressure, causing the pans to burst.

An alternative method to determine the enthalpy of fusion is to use the difference between the vapor pressures of the solid and of the liquid, because the difference in enthalpy must be the same going from one state to another, disregarding how the second state is reached. A large vapor-pressure data-set is available for D-camphor (for a plot cf. supplementary materials), extending over the liquid phase, the cubic phase and the hexagonal phase [24]. Surprisingly, vapor-pressure data compiled by Boublik [25], copied from [24], are related to a unique "crystalline" solid, thus as if phase changes in the solid state would have no influence on the vapor pressure. In the present analysis, the phase changes have been taken into account. Other literature data coincide with De Wilde's data, but contain much less points [26–29]. Fitting the data of De Wilde [24] to the following equation, assuming $\Delta_{\alpha}^{vap}H$

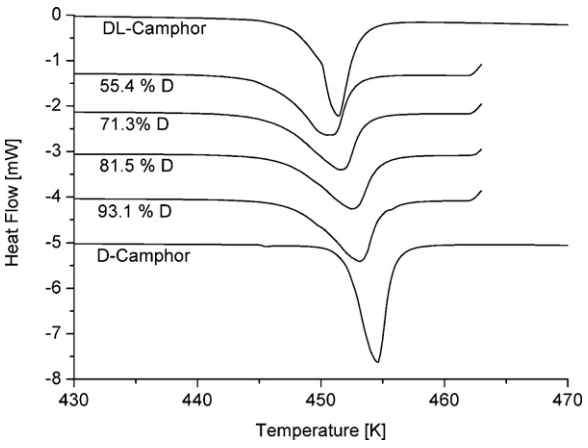

Fig. 5. DSC-curves of fusion of D-DL-camphor mixtures with curves for D-camphor (100%), bottom, and DL-camphor (50%), top. The curves have been normalized reflecting a 1 mg quantity and shifted along the *y*-axis to facilitate comparison. The peaks represent endothermic transitions. The melting points obtained from these curves have been plotted in Fig. 6.

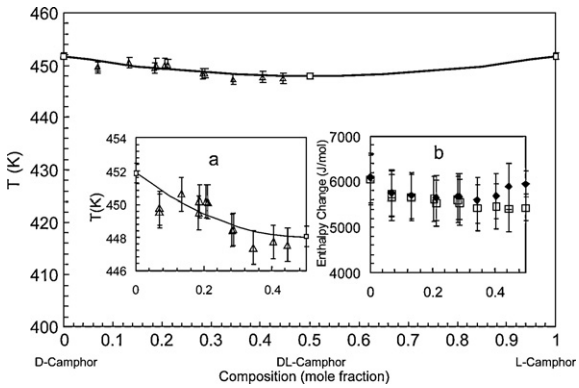

Fig. 6. The *T*–*X* phase diagram of D- and L-camphor at the transition I → L. '△' are the transition temperatures of mixtures and '□' the onset temperatures of the melting points of D-, L-, and DL-camphor (Table 4). Inset a: close-up of the data points. Inset b: transition enthalpy as a function of composition, '♦' melting enthalpy and '□' crystallization enthalpy changes. The solid line is the equal-G curve for mixed crystals between D- and L-camphor; due to the small differences in melting temperature the solidus and liquidus lines will be found close to the equal-G curve.

independent of temperature:

$$\ln p = \frac{-\Delta_{\alpha}^{\mathrm{vap}}H}{RT} + b \tag{1}$$

with p the pressure, $\Delta_{\alpha}^{\mathrm{vap}}H$ (α = L) the enthalpy of vaporization and $\Delta_{\alpha}^{\mathrm{vap}}H$ for enthalpy of sublimation (α = solid phase), R the gas constant, T the temperature and b a constant. This results in a vaporization enthalpy $\Delta_{\mathrm{L}}^{\mathrm{vap}}H$ of 44.4 ± 0.2 kJ mol^{-1} and an enthalpy of sublimation for the cubic phase $\Delta_{\mathrm{I}}^{\mathrm{vap}}H$ of 50.9 ± 0.1 kJ mol^{-1}; thus, the enthalpy of fusion is the difference $\Delta_{\mathrm{I}}^{\mathrm{L}}H$ 6.5 ± 0.3 kJ mol^{-1}, which corresponds well with the values determined by DSC (Table 4). In the same manner, the values for the II–I transition have been determined, but due to the low vapor pressure for the hexagonal phase and the small transition enthalpy, the uncertainty is as large as the values themselves (cf. Table 2).

3.3. Temperature–composition phase diagram at the melting point

The data presented above, concerning pure D-camphor and racemic camphor, can be used to predict the melting behavior through the entire composition range of the phase diagram. But first the basic type of phase diagram has to be determined, which for enantiomer systems can be: conglomerates, giving rise to a eutectic transition, racemic compounds (racemate) or mixed crystals (solid solutions) [30,31]. The melting behavior was studied for a number of D- and DL-camphor mixtures and the melting temperatures were obtained from DSC-curves following a procedure described in the literature [31]; a number of representative curves can be found in Fig. 5 and the resulting section of the phase diagram in Fig. 6.

The lack of a eutectic transition rules out the existence of conglomerates (or mixtures) consisting of the cubic phases of D- and L-camphor. Thus, the phase diagram depicts either of two ideal cases. (1) A continuous solid solution of D- and L-camphor, where DL-camphor represents one of the many randomly distributed mixtures within a continuum or (2) a limited solid solution between enantiomer and racemic compound; the latter must have a different space group, which contains a mirror plane not found for the enantiomer. In the latter case, a two-phase region must exist between the enantiomer-based solid solution and the pure racemic compound. The question is, however, if any method that provides a time- or space-averaged image of the system can distinguish between the racemic compound and a randomly distributed solid solution. Disregarding positional disorder, which must be extensive given that it exists in the low temperature phase, orientational disorder renders camphor molecules near spherical. This means that it becomes impossible to recognize right-handed from left-handed in a time- or space-averaged image, in other words the effective symmetry of a racemic compound and of a random solid solution have become equivalent. One could call this a case of 'critical symmetry'.

A thermodynamic assessment of the melt equilibrium was carried out by means of the EGC method (EGC: 'equal Gibbs-energy curve' is a line in between the solidus and liquidus, indicating the global composition where the difference in Gibbs energy between two phases in equilibrium is zero) [32]. The Gibbs energy for a mixture of $(1-X)$ mol of pure component A and X mol of pure component B displaying isomorphism in solid phase α can be written as a function of temperature and composition:

$$G^{\alpha}(T,X) = (1-X)\mu_{\mathrm{A}}^{*,\alpha} + X\mu_{\mathrm{B}}^{*,\alpha} + RTLN(X) + G^{\mathrm{E},\alpha}(T,X) \tag{2}$$

where $\mu_i^{*,\alpha}$, i = A or B, represent the molar Gibbs energies of pure components A and B, R is the gas constant, $LN(X) = (1-X)\ln(1-X) + X\ln X$ and $G^{\mathrm{E},\alpha}(T,X)$ is the excess Gibbs energy accounting for deviation from ideal behavior of the mixture in form α (assuming an excess Gibbs energy of zero for the melt, i.e. an ideal mixed liquid phase). The two-phase equilibrium region [α + L] is given by the common tangent between the Gibbs energies $G^{\alpha}(T,X)$ and $G^{\mathrm{L}}(T,X)$ as a function of T. In the case of insufficient data on ${\mu_i}^{*,j}$ i = A,B and j = α,L, the simplified treatment of the equal Gibbs curve (EGC) method can be used.

The difference between the Gibbs energies of the α and L phase is given by:

$$\begin{aligned}\Delta_{\alpha}^{\mathrm{L}}G(T,X) &= G^{\mathrm{L}}(T,X) - G^{\alpha}(T,X) \\ &= (1-X)\Delta_{\alpha}^{\mathrm{L}}\mu_{\mathrm{A}}^{*}(T) + X\Delta_{\alpha}^{\mathrm{L}}\mu_{\mathrm{B}}^{*}(T) + \Delta_{\alpha}^{\mathrm{L}}G^{\mathrm{E}}(T,X)\end{aligned} \tag{3}$$

where $\Delta_{\alpha}^{\mathrm{L}}\mu_i^{*}(T)$ is $\mu_i^{*,\mathrm{L}} - \mu_i^{*,\alpha}$ (i = A,B) and $\Delta_{\alpha}^{\mathrm{L}}G^{\mathrm{E}}(T,X)$ is the excess Gibbs-energy difference between the considered phases $G^{\mathrm{E,L}}(T,X) - G^{\mathrm{E},\alpha}(T,X)$. Assuming that the specific heat does not change significantly in the studied temperature range $\Delta_{\alpha}^{\mathrm{L}}\mu_i(T) \approx \Delta_{\alpha}^{\mathrm{L}}S_i \cdot (T_i^{\alpha\to\mathrm{L}} - T)$, where $\Delta_{\alpha}^{\mathrm{L}}S_i$ is the melting entropy and $T_i^{\alpha\to\mathrm{L}}$ is the melting temperature of phase α. Eq. (3) equals zero if $G^{\mathrm{L}}(T,X)$ and $G^{\alpha}(T,X)$ are equal, which for each mole fraction occurs at a specific, equilibrium defined, temperature, the EGC-temperature. Thus, $\Delta_{\alpha}^{\mathrm{L}}G(T_{\mathrm{EGC}}, X_{\mathrm{EGC}}) = 0$, gives rise to the EGC-curve in the *T*–*X*

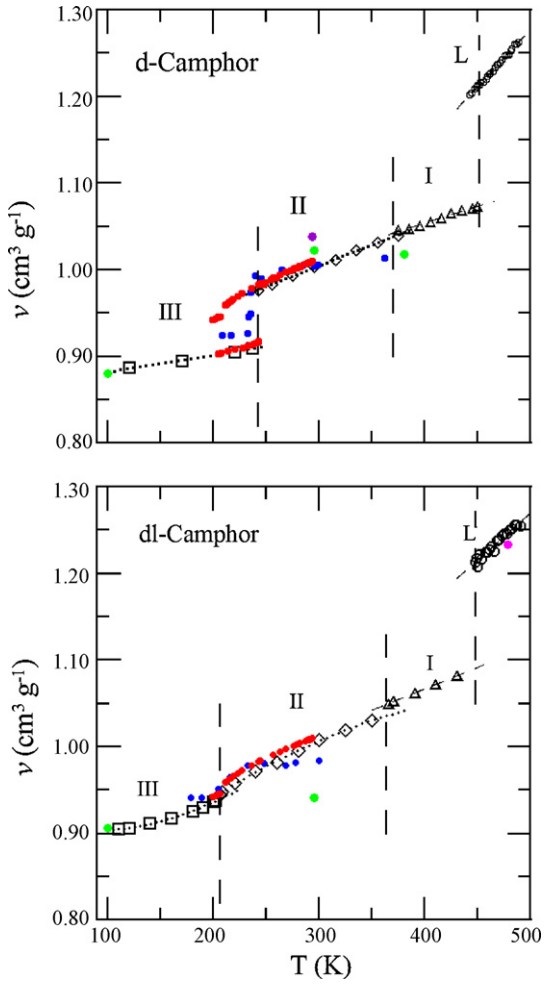

Fig. 7. Specific volume of D-camphor (upper panel) and DL-camphor (lower panel) as a function of temperature for phases III (open squares), II (open diamonds), I (open triangles) and liquid (open circles). Literature values are presented with solid circles: blue for White and Morgan [33], red for Schäfer et al. [5,6], magenta for Malosse [35], violet for Kuhara [34] and green for lattice parameters by Mjojo [3] and Brunelli et al. [12]. (For interpretation of the references to color in this figure legend, the reader is referred to the web version of the article.)

plane given by the expression:

$$T_{EGC}(X) = \frac{(1-X)\Delta^{L}_{\alpha}H_A + X\Delta^{L}_{\alpha}H_B}{(1-X)\Delta^{L}_{\alpha}S_A + X\Delta^{L}_{\alpha}S_B} + \frac{\Delta^{L}_{\alpha}G^{E}_{EGC}(X)}{(1-X)\Delta^{L}_{\alpha}S_A + X\Delta^{L}_{\alpha}S_B} \quad (4)$$

where $\Delta^{L}_{\alpha}H_i$, i = A,B stands for the melting enthalpy of pure component i. The first term of the right side of Eq. (4) represents the EGC-temperature for the [α + L] equilibrium when the excess Gibbs-energy difference is zero and is only pure component-dependent. The second term depends on the excess Gibbs-energy difference along the EGC-curve.

Using the experimental data (solidus or liquidus) corresponding to each equilibrium, the excess Gibbs-energy difference related to the EGC-curve, $\Delta^{L}_{\alpha}G^{E}_{EGC}(X)$, is found. The excess Gibbs difference can be represented by a one-parameter Redlich–Kister polynomial, because for mixtures of optical antipodes the asymmetry term should be zero, and thus:

$$\Delta^{L}_{\alpha}G^{E}_{EGC}(X) = X(1-X)\left(\Delta^{L}_{\alpha}G_1\right) \quad (5)$$

where the parameter $\Delta^{L}_{\alpha}G_1$ expresses the magnitude of the excess Gibbs-energy difference at equimolar composition. It should be noted that Eq. (5) provides an excess Gibbs-energy difference independent of temperature, but its value is highly linked with the temperature range of the input data.

In the case of a binary mixture of a pair of enantiomers, the first term of Eq. (4) will be the melting temperature of the pure enantiomer independent of composition. Any deviation from this horizontal line, as in the case of DL-camphor (X = 0.5), must be accounted for by the second term. That means that with the entropy of fusion of the pure enantiomer ($\Delta^{L}_{I}S_{d\text{-camphor}} = \Delta^{L}_{I}S_{l\text{-camphor}}$) and the melting point of the racemic mixture (X = 0.5) a relation for $\Delta^{L}_{I}G^{E}_{EGC}(X)$ can be obtained, which can be described by Eq. (5) or even more simple, $\Delta^{L}_{I}G^{E}_{EGC}(0.5)$ can be calculated directly. Using the values from Table 4 and the fact that $\Delta_f S = \Delta_f H/T_f$, this leads to a value for $\Delta^{L}_{I}G^{E}_{EGC}(0.5) = -53\,J\,mol^{-1}$. If it is assumed that the excess Gibbs energy is zero for the liquid phase, which is likely for the almost spherical camphor enantiomers, the excess Gibbs energy of the racemic mixture $G^{I,E}_{EGC}(0.5)$ must be $53\,J\,mol^{-1}$. A similar calculation can be performed for the solid–solid transition II–I. With the values from Table 4, the following result was found $\Delta^{I}_{II}G^{E}_{EGC}(0.5) = -2.6\,J\,mol^{-1}$. There is an additional $2.6\,J\,mol^{-1}$ Gibbs-energy gain for DL-camphor to transform from hexagonal into the cubic structure in comparison to ideally mixed enantiomers and then $G^{II,E}_{EGC}(0.5) = 56\,J\,mol^{-1}$.

For both excess Gibbs-energy differences, the values are small, indicating that the characteristics of phase I and II of DL-camphor are close to those of ideal solid solutions and hence that a racemic compound, if it exists in the binary system, must be thermodynamically very similar to an ideal solid solution. The latter conclusion is corroborated by the observation that the EGC and the melting points as a function of composition in the inset in Fig. 6 coincide within error.

3.4. Specific volume of camphor as a function of temperature

The specific volume of D-camphor, the pure enantiomer, is considerably smaller than the volume of DL-camphor in phase III; a

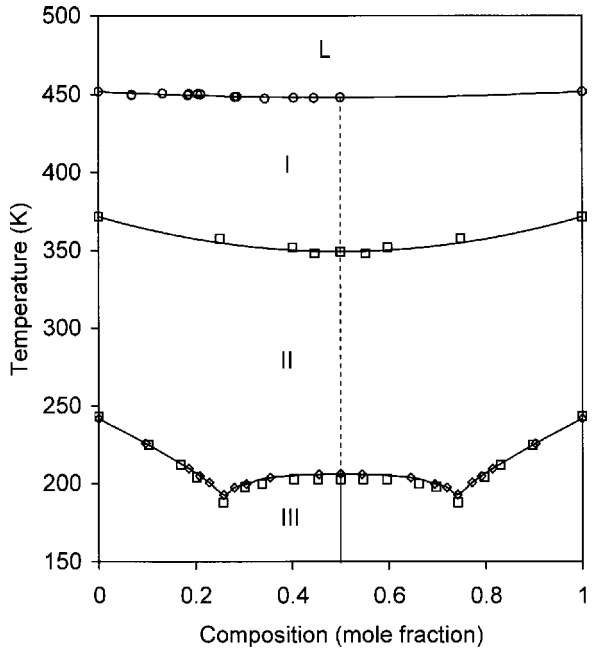

Fig. 8. Phase diagram of D-camphor and L-camphor. Phase III consists of orthorhombic crystalline phases, which for the racemic compound is positionally disordered. Phase II and I are solid solutions with, respectively, a hexagonal and a face-centered cubic structure. The structure of a possible racemic compound would be effectively equivalent to a solid solution, because of the plastic phase. Thus, one can consider phase II and I as a continuum of solid solutions between both enantiomers.

result, which is confirmed by independent X-ray measurements (Fig. 7) [8,12]. The temperatures for the III → II transition are found to be in accordance with the DSC data. The volumes at room temperature are the same within error for D- and DL-camphor. Determination of the volume-composition phase diagram of camphor resulted in a minute difference of 1.3 Å^3 between 511.1 Å^3 for DL-camphor and 509.8 Å^3 for D-camphor (cf. supplementary material Fig. S2), thus equal within error. Literature corresponds to the present findings. The only significant deviations are the specific volume of DL-camphor by White and Morgan [33] and the value published by Mjojo for DL-camphor [3].

At higher temperature, the present experiments indicate that in phase I, the volumes of D- and DL-camphor are similar. They are higher than the volumes published by Mjojo and White and Morgan [3,33]. For the liquid phase the specific volumes are the same; the single value found by Kuhara [34] is close to the new data published in this paper. Malosse once presented a specific volume obtained from solution for – unidentified – camphor. This value appears to be an overestimate compared to all the other available data [35].

4. Conclusion

The melting temperatures of D-camphor and DL-camphor were found to be 451.8 ± 0.7 K and 448.0 ± 0.7 K, respectively. Compared to the literature averages, the present values fall well within the uncertainty ranges and they demonstrate a difference in melting temperature between pure and racemic camphor of about 2–3 K. Taking literature into account, the expected average melting points for D- and DL-camphor become 451 ± 2 K and 449 ± 2 K, but this should include a difference between the two values of at least 2 K.

For the enthalpies of fusion, it is more difficult to obtain values with a narrow uncertainty range due to the erratic behavior of in particular D-camphor during fusion. It can be seen in Fig. 3 and Table 4 that at low V/m the measured enthalpy of fusion is as erratic as the average over the literature data. The cause is unknown, but may have to do with disorder, the nature of plastic crystals and high vapor pressure. The value found in this paper for the enthalpy of fusion for D-camphor is equal to the literature average 6.2 ± 0.6 kJ mol^{-1}. For DL-camphor the value found in this paper is 5.9 ± 0.3 kJ mol^{-1}, which is lower than the value for D-camphor, whereas from the literature an average higher than D-camphor is found. Thus, it can be concluded that the enthalpies of D- and DL-camphor are the same within error.

The specific volume of the racemic mixture in phase III exhibits a large excess in comparison to the pure enantiomer. This is in accordance with the literature, where disorder and metastability have been demonstrated indisputably [4,8]. Furthermore, the second order appearance of the transition from phase III → II for the racemic mixture demonstrated in the literature [4,8], is observed in the present specific volume data too. The specific volumes for phase II, I, and liquid are equal or similar for D- and DL-camphor and in combination with the literature data, the volume of camphor as a function of temperature is now well established.

The T–X phase diagram between the optical antipodes D- and L-camphor has been expanded to the melting transition (Fig. 8). The existence of a racemic compound has been confirmed for phase III by a crystal structure different from that of the pure enantiomer [8,12]. Whether phase I consists of solid solution between D-camphor and L-camphor, as usually assumed, or between D-camphor and a racemic compound cannot be determined with DSC measurements nor with X-ray powder diffraction. However, the question may not be valid as orientational disorder will cause the apparent symmetry of both the racemic compound and a random solid solution to become equivalent, a case of so-called critical symmetry.

Acknowledgements

The authors thank H. Szwarc for sharing his views about the camphor system. R.C. acknowledges an invited position from the Generalitat de Catalunya (2007PIV0011) at the Universitat Politècnica de Catalunya. This work was partially supported by the Spanish Grant FIS2008-00837 and by Grant 2009SGR-1251 from the Catalan Government.

Appendix A. Supplementary data

Supplementary data associated with this article can be found, in the online version, at doi:10.1016/j.tca.2010.07.023.

References

[1] J. Jacques, A. Collet, S.H. Wilen, Enantiomers, Racemates and Resolutions, John Wiley & Sons, New York, 1981.
[2] J.E. Anderson, W.P. Slichter, J. Chem. Phys. 41 (1964) 1922–1928.
[3] C.C. Mjojo, J. Chem. Soc., Faraday Trans. II (1979) 692–703.
[4] T. Nagumo, T. Matsuo, H. Suga, Thermochim. Acta 139 (1989) 121–132.
[5] K. Schäfer, O. Frey, Z. Elektrochem. 56 (1952) 882–889.
[6] K. Schäfer, U. Wagner, Z. Elektrochem. 62 (1958) 328–335.
[7] C.C. Mjojo, H.K. Welsh, J. Chem. Soc., Faraday Trans. 88 (1992) 2909–2913.
[8] A.J. Mora, A.N. Fitch, J. Solid State Chem. 134 (1997) 211–214.
[9] G.B. Kauffman, J. Chem. Educ. 60 (1983) 341.
[10] F. Wallerant, C. R. Acad. Sci., Ser. II Univers. 158 (1914) 597–598.
[11] O. Andersson, R.G. Ross, A. Jezowski, Mol. Phys. 70 (1990) 1065–1083.
[12] M. Brunelli, A.N. Fitch, A.J. Mora, J. Solid State Chem. 163 (2002) 253–258.
[13] V.T. Witusiewicz, L. Sturz, U. Hecht, S. Rex, Acta Mater. 52 (2004) 4561–4571.
[14] J.R. Donnelly, L.A. Drewers, R.L. Johnson, W.D. Munslow, K.K. Knapp, G.W. Sovocool, Thermochim. Acta 167 (1990) 155–187.
[15] J.D.M. Ross, I.C. Somerville, J. Chem. Soc. (1926) 2770–2784.
[16] V.K. Abrosimov, V.I. Smirnov, V.A. Kuznetsov, T.M. Okhrimenko, E.P. Efremova, Russ. J. Phys. Chem. 77 (2003) 1191–1193.
[17] P. Espeau, R. Céolin, Thermochim. Acta 376 (2001) 147–154.
[18] J.-C. Rouland, R. Céolin, C. Souleau, P. Khodadad, J. Therm. Anal. 23 (1982) 143.
[19] R.C. Weast, M.J. Astle, W.H. Beyer (Eds.), CRC Handbook of Chemistry and Physics, 67th ed., CRC Press, Boca Raton, 1986.
[20] J. Ballon, V. Comparat, J. Pouxe, Nucl. Instrum. Methods Phys. Res., Sect. A 217 (1983) 213–216.
[21] M. Evain, P. Deniard, A. Jouanneaux, R. Brec, J. Appl. Crystallogr. 26 (1993) 563.
[22] J. Rodriguez-Carvajal, Commission on Powder Diffraction (IUCr) Newsletter 26 (2001) 12–19.
[23] P. Espeau, R. Céolin, Thermochim. Acta 445 (2006) 32–35.
[24] J.H. De Wilde, Z. Anorg. Allg. Chem. 233 (1937) 411–414.
[25] T. Boublik, V. Fried, E. Hala, The Vapor Pressures of Pure Substances, Elsevier, Amsterdam, 1973.
[26] R.W. Allen, J. Chem. Soc., Trans. 77 (1900) 413.
[27] F. Förster, Ber. Dtsch. Chem. Ges. 23 (1890) 2981.
[28] W. Ramsay, S. Young, Philos. Trans. R. Soc. Lond. 175 (1884) 45.
[29] E. Vanstone, J. Chem. Soc., Trans. 97 (1910) 429–443.
[30] H.W. Bakhuis Roozeboom, Z. Phys. Chem. Stoechiom. Verwandtschafts 28 (1899) 494–517.
[31] H.E. Gallis, F. Bougrioua, H.A.J. Oonk, P.J. Van Ekeren, J.C. Van Miltenburg, Thermochim. Acta 274 (1996) 231–242.
[32] H.A.J. Oonk, Phase Theory, The Thermodynamics of Heterogeneous Equilibria, Elsevier, Amsterdam, 1981.
[33] A.H. White, S.O. Morgan, J. Am. Chem. Soc. 57 (1935) 2078–2086.
[34] M. Kuhara, Am. Chem. J. 11 (1889) 244–248.
[35] H. Malosse, C. R. Acad. Sci., Ser. II Univers. 154 (1912) 1697–1698.
[36] G.A. Hulett, Z. Phys. Chem. (Munich) 28 (1899) 629–672.
[37] P.W. Bridgman, Proc. Am. Acad. Art. Sci. 52 (1916) 91–187.
[38] Landolt Bornstein, New Series Group IV, Thermodynamic Properties of Organic Compounds and Their Mixtures. Subvol. A. Enthalpies of Fusion and Transformation of Organic Compounds, vol. 8, Springer, Berlin, 1995.
[39] K. Schäfer, An. R. Soc. Esp. Fys. Quim. B Quim. 49B (1953) 161–174.
[40] K. Schäfer, U. Wagner, H. Engelbach, Chem. Ber. 89 (1956) 327–334.
[41] D.E. Williams, C.P. Smyth, J. Am. Chem. Soc. 84 (1962) 1808–1812.
[42] P.M. Robinson, H.J. Rossell, H.G. Scott, Mol. Cryst. Liq. Cryst. 10 (1970) 61.
[43] K. Sekiguchi, Y. Tsuda, K. Chihara, E. Suzuki, Yakugaku Zasshi 103 (1983) 213–224.
[44] T. Sato, W. Kurz, K. Ikawa, Trans. Jpn. Inst. Met. 28 (1987) 1012.
[45] H. Hamada, Bull. Chem. Soc. Jpn. 61 (1988) 869–878.
[46] T. Taenaka, H. Esaka, S. Mizoguchi, H. Kajioka, Mater. Trans. JIM 30 (1989) 360–364.
[47] M. Frandsen, Bur. Stand. J. Res. 7 (1931) 477–483.
[48] J.G. Aston, in: D. Fox, M.M. Labes, A. Weissember (Eds.), Physics and Chemistry of Organic Solid State, vol. 1, Interscience Publ., New York, 1963, p. 543.